Supplementary Materials

Fast Redox Conversion in Lithium-Sulfur Batteries Enabled by Cu-doped $W_{18}O_{49}$ with Abundant Oxygen Defects

Guilin Meng[a,c,#], Guojun Dong[b#], Yanfei Yang[a,], Yingpu Bi[b,c,*] and Junping Zhang[a,c,*]*

[a] Center of Eco-Material and Green Chemistry, Lanzhou Institute of Chemical Physics, Chinese Academy of Sciences, Lanzhou 730000, P.R. China. E-mail: yangyf@licp.cas.cn (Y. F. Yang); jpzhang@licp.cas.cn (J. P. Zhang)

[b] State Key Laboratory for Oxo Synthesis & Selective Oxidation, National Engineering Research Center for Fine Petrochemical Intermediates, Lanzhou Institute of Chemical Physics, Chinese Academy of Sciences, Lanzhou 730000, P.R. China. E-mail: yingpubi@licp.cas.cn (Y. P. Bi)

[c] Center of Materials Science and Optoelectronics Engineering, University of Chinese Academy of Sciences, Beijing 100049, P.R. China

[#] These authors contributed equally to this work.

Experimental Section

1.1 Materials

Tungsten chloride (WCl_6, 99.9%), copper nitrate ($Cu(NO_3)_2$, 99.9%), nano S powder, and Li_2S were purchased from Sigma-Aldrich (Shanghai) Co., Ltd. Anhydrous ethanol (EtOH, 99.5%) and methanol (99.9%) were purchased from Tianjin Kemiou Chemical Reagent Co., Ltd., China. Polypropylene separator (PP, Celgard2500), carbon coated Al foil, Super P, NMP and Li metal anode were purchased from Guangdong Canrd New Energy Technology Co., Ltd., China. Liquid electrolytes were purchased from DodoChem, China. Carbon nanotubes (CNT, Tube8©) were purchased from JENO, Korea.

1.2 Preparation of CNT/S cathodes

The CNT/S composite was prepared using a conventional melt-diffusion method. Typically, CNT and S with a mass ratio of 2:8 were well ground and heated at 155 °C for 12 h under N_2 atmosphere to generate the CNT/S composite. The S content in the CNTs/S composite was 80% as confirmed in our previous work.[1]

The CNT/S cathodes were prepared by a simple coating method, in which 80 wt% of the CNT/S composite, 10 wt% of Super P, and 10 wt% of PVDF were homogeneously mixed in NMP and cast onto carbon-coated Al foil. The CNT/S cathodes were dried at 60 °C for 12 h under vacuum, and then cut into circular disks with a diameter of 14 mm for the battery assembly. The S mass loading in the cathode is about 1.2 mg cm^{-2}.

1.3 Assembly and electrochemical tests of the Li//S batteries

CR2032 coin cells were used to assemble Li//S batteries in an Ar-filled glovebox with O_2 and H_2O contents below 0.1 ppm. The Li//S batteries were assembled with the CNT/S cathode, separator, and the Li anode (400 μm). The 1 M LiTFSI and 2% $LiNO_3$ dissolved in DOL/DME (v:v = 1:1) was used as electrolyte. The ratio of electrolyte to S (E/S) is about 15 μL mg^{-1}.

A CT2001A battery test system (LAND Electronic Co., China) was used to study the rate performances and cycling stabilities of the Li//S batteries with a voltage range of 1.7-2.8 V at various rates. The CV and electrochemical impedance spectroscopy (EIS) were collected using an electrochemical working station (CHI660E).

The LiPS inhibiting capability of separators was studied by shuttle current of the Li//S batteries without $LiNO_3$. After 3 cycles, the Li//S battery was discharged to 2.38 V, and then tuned to the potentiostatic mode. The shuttle current was recorded after 10,000 s.

1.4 Measurement of self-discharge behaviors

A CT2001A battery test system (LAND Electronic Co., China) was used to study the self-discharge behaviors of Li//S batteries. After 10 cycles, the batteries were discharged to 2.1 V at the 11^{th} cycle and rested for 7 d, and then the batteries were tuned on normal discharge-charge cycle. The Li//S batteries were assembled with the CNT/S cathode, separator, and the Li anode (400 μm). The 1 M LiTFSI and 2% $LiNO_3$ dissolved in DOL/DME (v:v = 1:1) was used as electrolyte.

1.5 Measurement of electrocatalytic activity

The electrocatalytic activity of the samples for LiPS was characterized by the CV and

EIS of symmetrical cells. An electrochemical working station was used to record CV curves at operating potentials of -1 to 1 V with different scanning rates and EIS plots at open circuit potential with a constant perturbation amplitude of 5 mV in the frequency of 0.1-100 kHz. The symmetrical cells were assembled with the $W_{18}O_{49}$ or $Cu/W_{18}O_{49}$ electrode (as the work and the counter electrode) and the PP separator.

The Tafel plots and linear sweep voltammetry (LSV) were also collected on an electrochemical working station. The cells were assembled with the working electrode, PP separators and Li anode.

The $Cu/W_{18}O_{49}$ electrode was prepared by a simple coating method, in which 70 wt% of $Cu/W_{18}O_{49}$, 20 wt% of Super P, and 10 wt% of PVDF were homogeneously mixed in NMP and cast onto Al foil. The electrodes were dried at 60 °C for 12 h under vacuum atmosphere, and then cut into circular disks with a diameter of 14 mm. For comparison, the $W_{18}O_{49}$ and pure Super P electrodes were also prepared using a similar method. The sample mass loading in the electrode is ca. 0.35 mg cm^{-2}. The electrolyte (30 μL) consisted of Li_2S_6 (0.2 M) dissolved in liquid electrolyte.

1.6 Measurement of adsorption performance

The adsorption performance of samples for LiPS was tested in Ar atmosphere using a UV-Vis spectrometer (Lambda 35, PerkinElmer, USA). The LiPS (mainly Li_2S_6) solution was prepared by dissolving Li_2S and S powder with a molar ratio of 1:5 in the DOL solvent by stirring for 48 h. 15 mg of the sample was added in 5 mL of the Li_2S_6 solution (10 mM). The mixture was vibrated at 150 rpm for 10 min, and then rested for 24 h. The concentration of residual Li_2S_6 in the supernatant solution was tested

using the UV-Vis spectrometer.

1.7 Measurement of ionic conductivity

The symmetric cells were assembled by sandwiching a separator between two stainless steel blocking electrodes. The electrolyte (30 μL) was 1 M LiTFSI and 2% $LiNO_3$ in DOL/DEM (v:v=1:1). The Nyquist plots were collected using an electrochemical working station (CHI660E) at open circuit potential with a constant perturbation amplitude of 5 mV at a frequency of 0.1-100 kHz. The ionic conductivity (σ, mS cm^{-1}) was calculated using the Nyquist plots according to Equation S1.

$$\sigma = L/(R \times A) \quad \text{(S1)}$$

where L is the thickness of the separator (cm), R is the resistance (Ω), and A is the area of the stainless steel electrode (cm^2).

1.8 Measurement of Li^+ ion diffusion coefficients

The Li^+ ion diffusion coefficients (D, cm^2 s^{-1}) were calculated based on the classical Randles-Sevcik equation (Equation S2).[2] The Li//S batteries with different separators were used to achieve peak currents (I_p, A) at different scan rates (v, V s^{-1}).

$$|I_p| = 2.69 \times 10^5 \times n^{3/2} \times A \times C \times D^{1/2} \times v^{1/2} \quad \text{(S2)}$$

where n is the number of electrons per specific reaction, A is the surface area of the electrode (cm^2), and C is the concentration of Li^+ ions in the electrolyte (mol L^{-1}).

1.9 Characterization

The surface morphology and elemental maps of the samples were recorded using a field emission SEM (JSM6701F, JEOL) and a field emission TEM (TECNAI-G2-F30, FEI). Before SEM observation, all samples were coated with a thin layer of gold film (ca. 7

nm in thickness). HADDF-STEM was also carried out on the TEM. The powder XRD analysis was performed using an X-ray power diffractometer with Cu anode (PAN alytical Co. X'pert PRO), running at 40 kV and 30 mA, scanning from 3° to 80° in 2ϑ at 10° s^{-1}. The XPS spectra of the samples were recorded using a VG ESCALAB 250 Xi spectrometer with a monochromated Al Kα X-ray radiation source and a hemispherical electron analyzer. The spectra were collected in the constant pass energy mode with a value of 100 eV, and all binding energies were calibrated using the C 1s peak at 284.6 eV as the reference. The Raman spectra of samples were recorded using a LabRAM HR Evolution Raman spectrophotometer with a 532 nm laser (HORIBA Jobin Yvon S.A.S. France). Electron paramagnetic resonance (EPR) spectra were recorded on an EMX EPR spectrometer (Bruker EMXPLUS, Germany). The contact angles of electrolyte (10 μL) on the separators was collected at 25 °C on a Contact Angle System OCA 20 (Dataphysics, Germany).

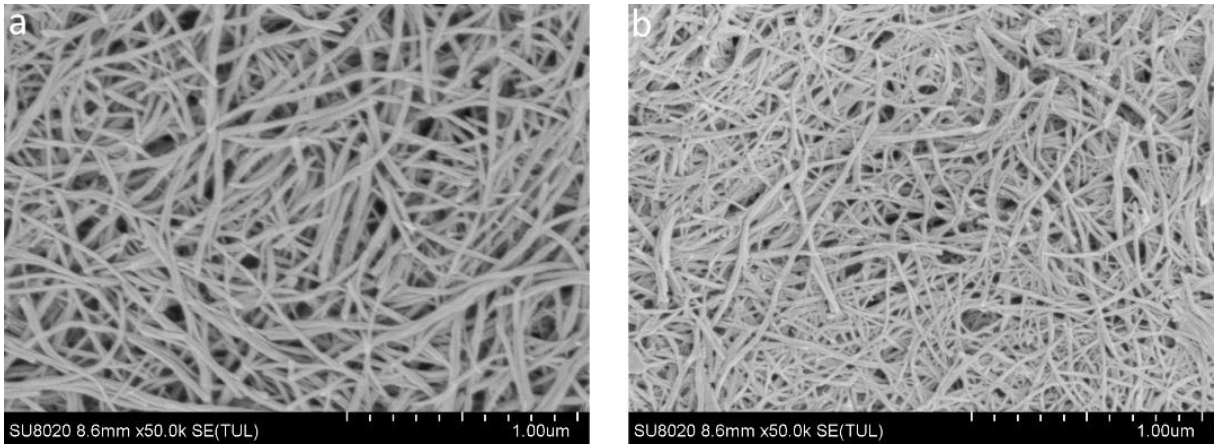

Fig. S1. SEM images of (a) $W_{18}O_{49}$ and (b) Cu/$W_{18}O_{49}$.

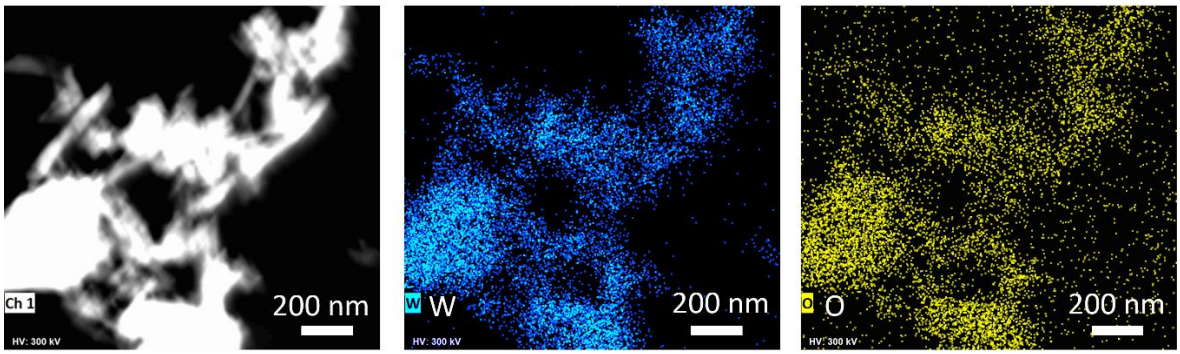

Fig. S2. Dark-field HADDF-STEM image and the corresponding elemental maps of $W_{18}O_{49}$.

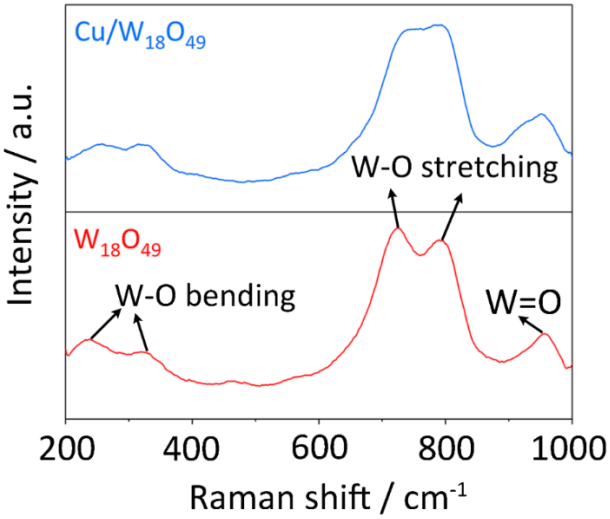

Fig. S3. Raman spectra of $W_{18}O_{49}$ and $Cu/W_{18}O_{49}$.

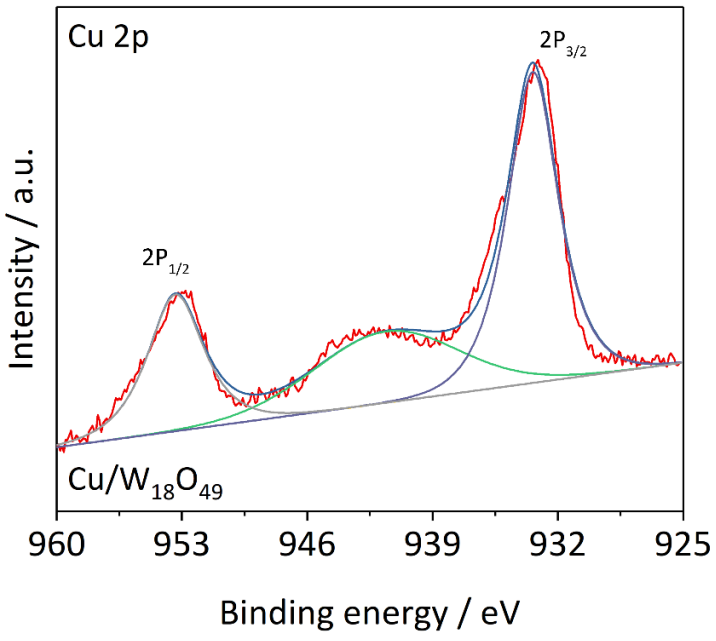

Fig. S4. High-resolution Cu 2p XPS spectrum of $Cu/W_{18}O_{49}$.

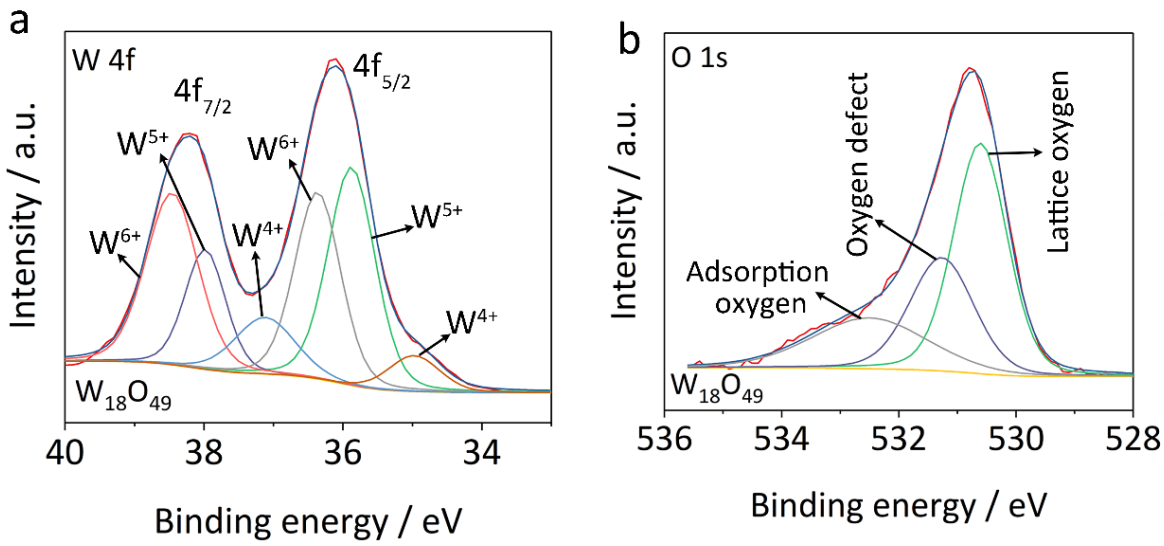

Fig. S5. High-resolution (a) W 4f and (b) O 1s XPS spectra of $W_{18}O_{49}$.

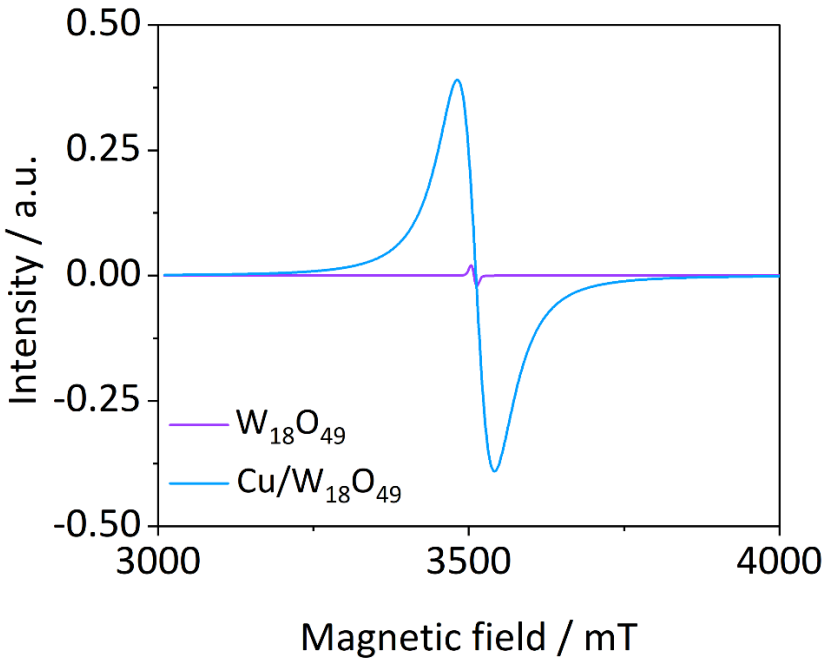

Fig. S6. EPR spectra of $W_{18}O_{49}$ and $Cu/W_{18}O_{49}$.

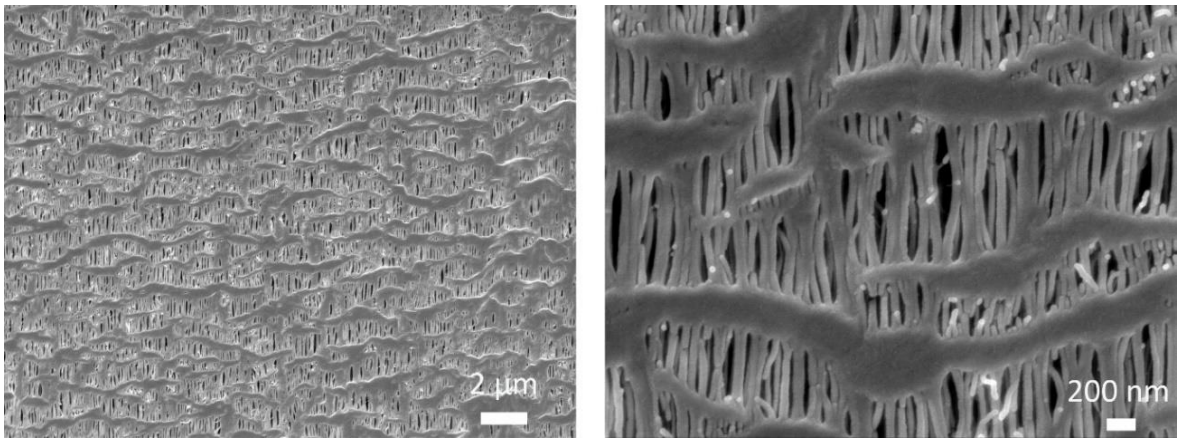

Fig. S7. SEM images of the PP separator.

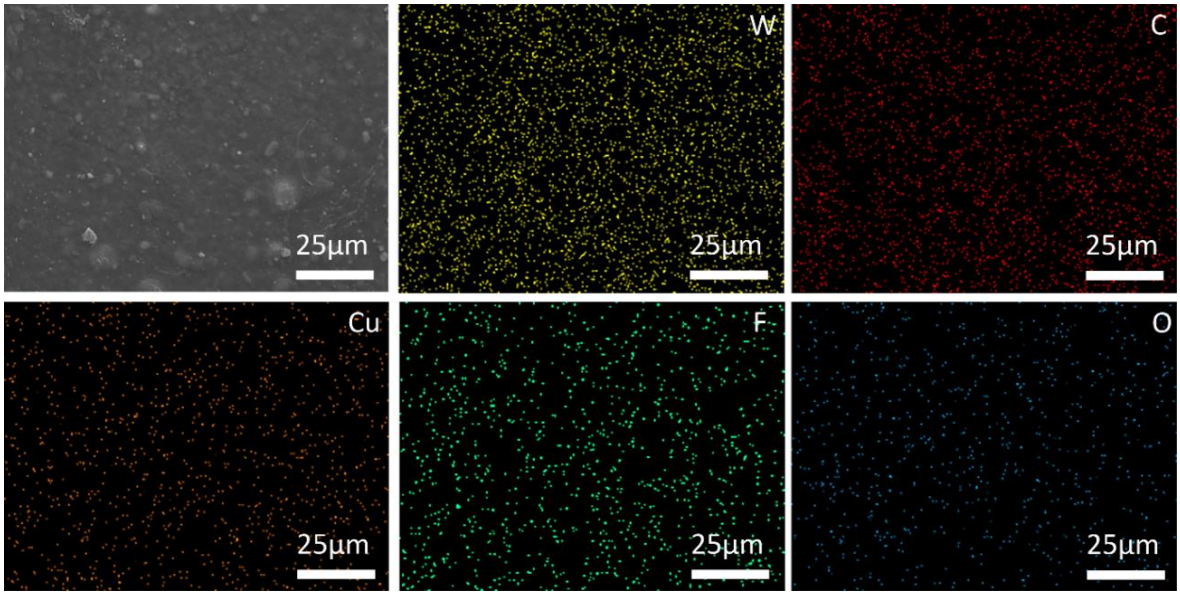

Fig. S8. Top-view SEM image and the corresponding elemental maps of the Cu/$W_{18}O_{49}$@PP separator.

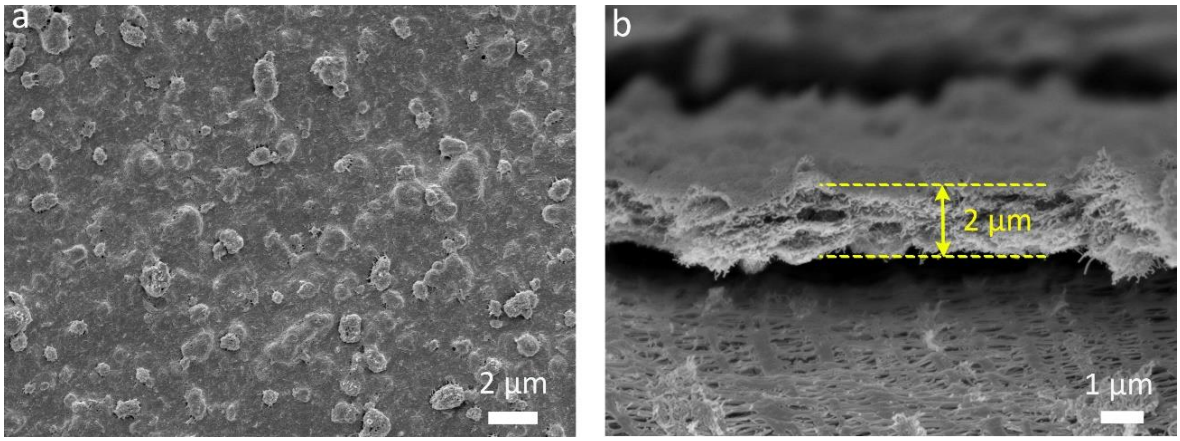

Fig. S9. (a) Top-view and (b) cross-sectional SEM images of the $W_{18}O_{49}$@PP separator.

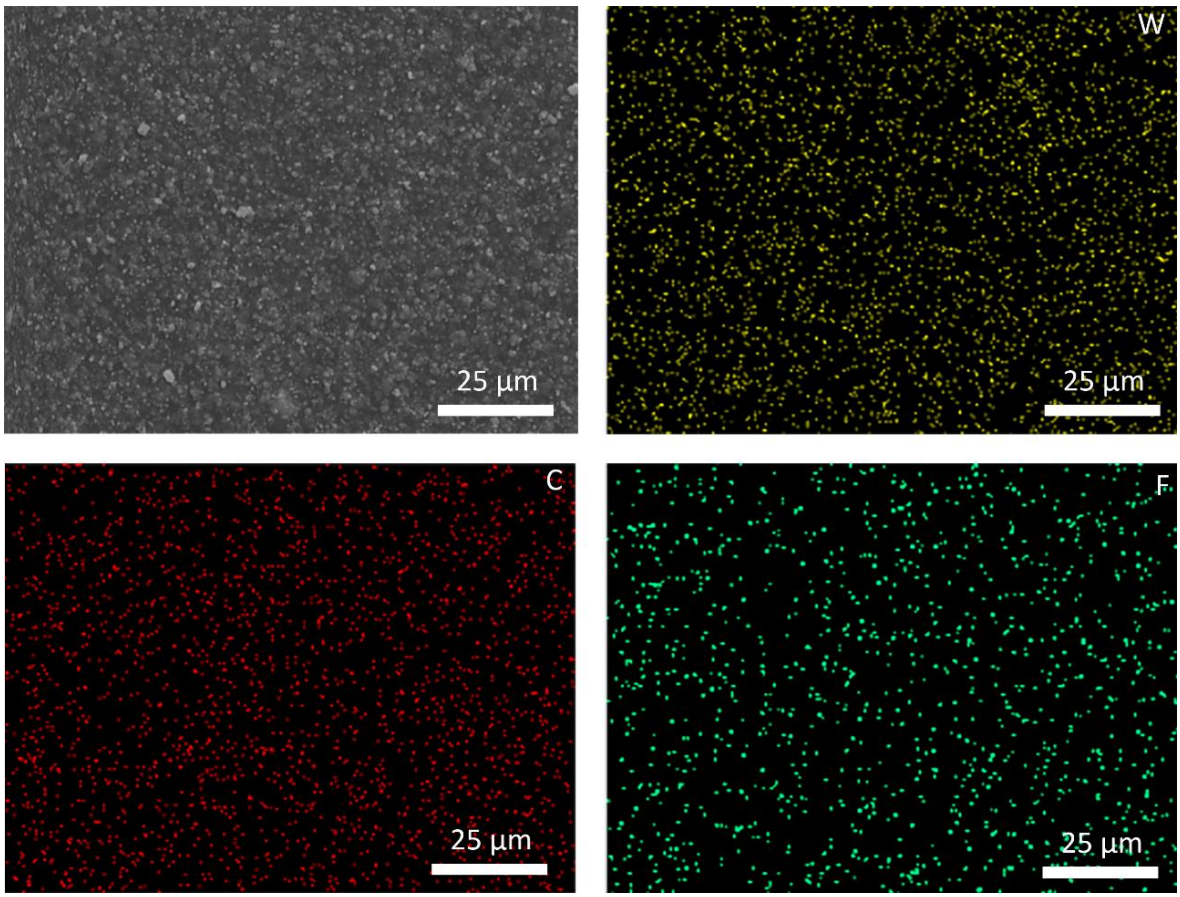

Fig. S10. Top-view SEM image and the corresponding elemental maps of the $W_{18}O_{49}$@PP separator.

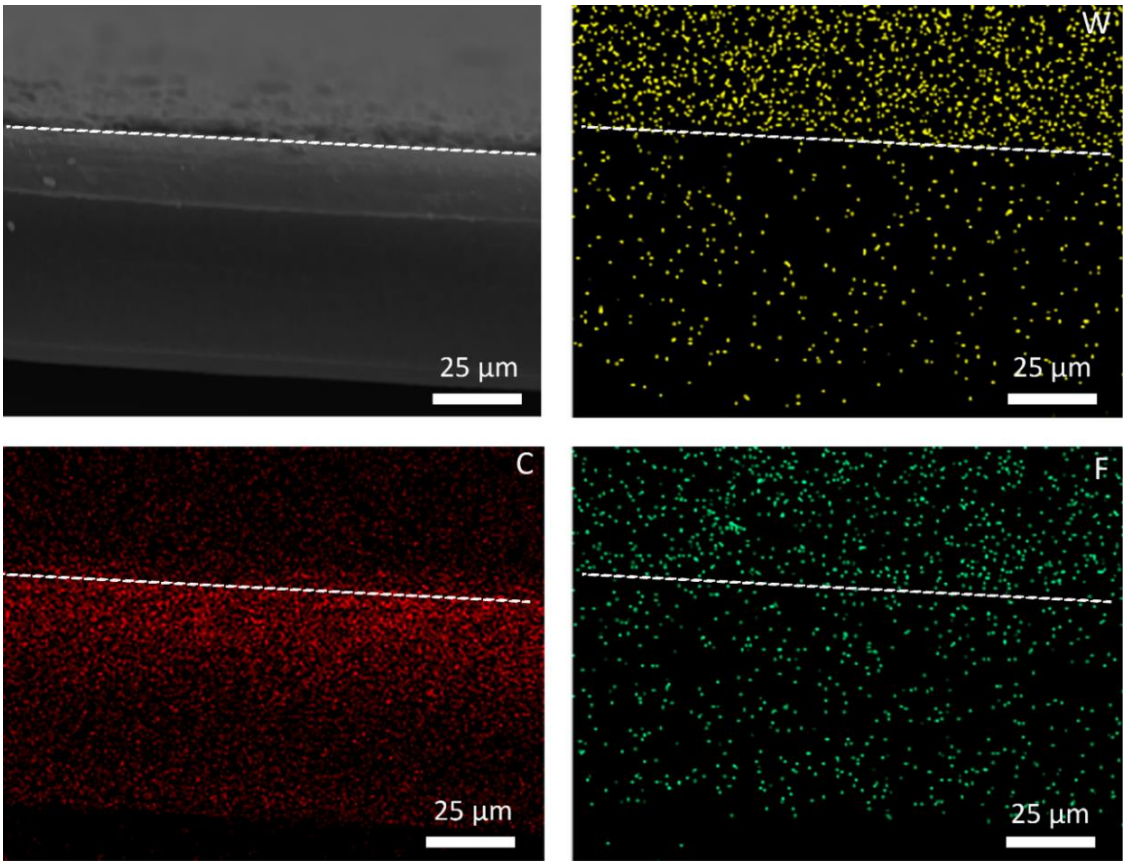

Fig. S11. Cross-sectional SEM image and the corresponding elemental maps of the $W_{18}O_{49}$@PP separator.

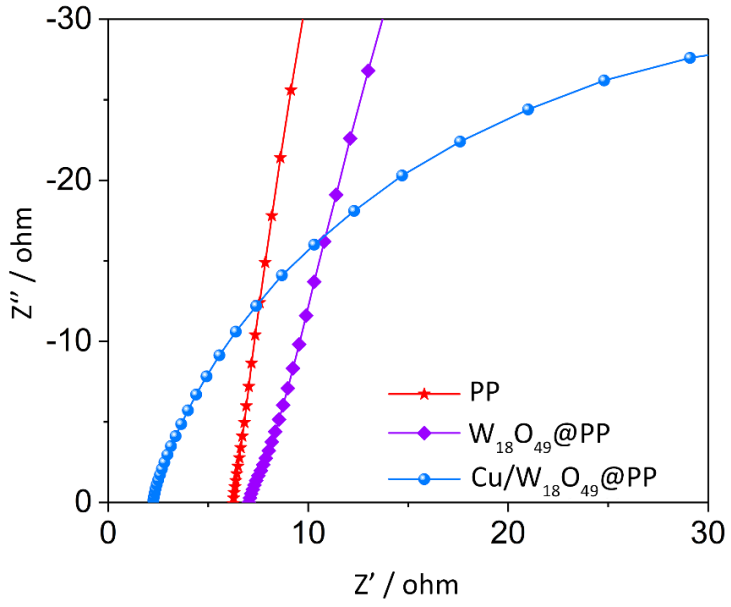

Fig. S12. EIS spectra of the cells with different separators for the calculation of ionic conductivity.

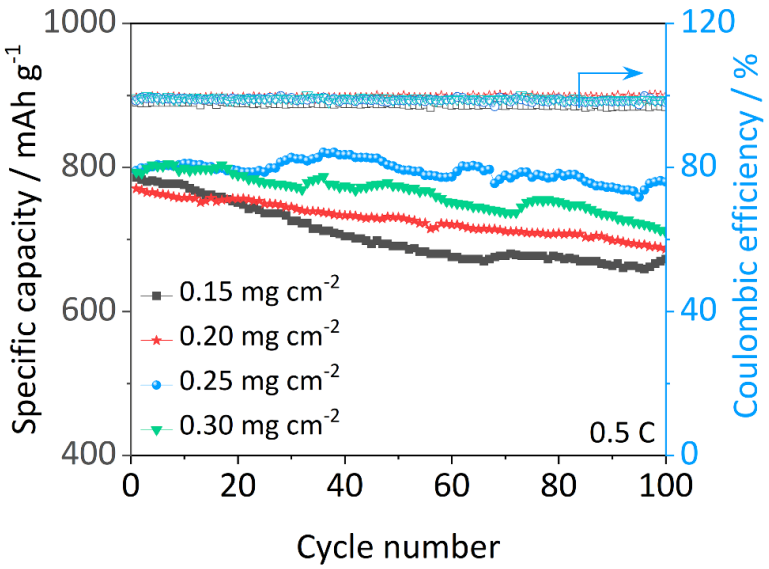

Fig. S13. Cycling stability of the Li//S batteries with the Cu/$W_{18}O_{49}$@PP separators with different Cu/$W_{18}O_{49}$ mass percentage.

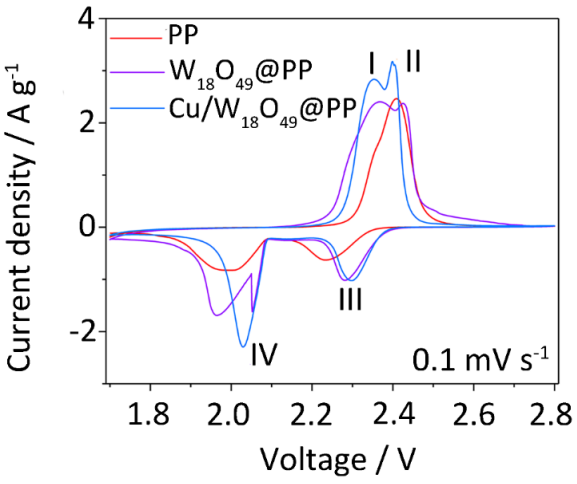

Fig. S14. CV curves of the Li//S batteries with different separators.

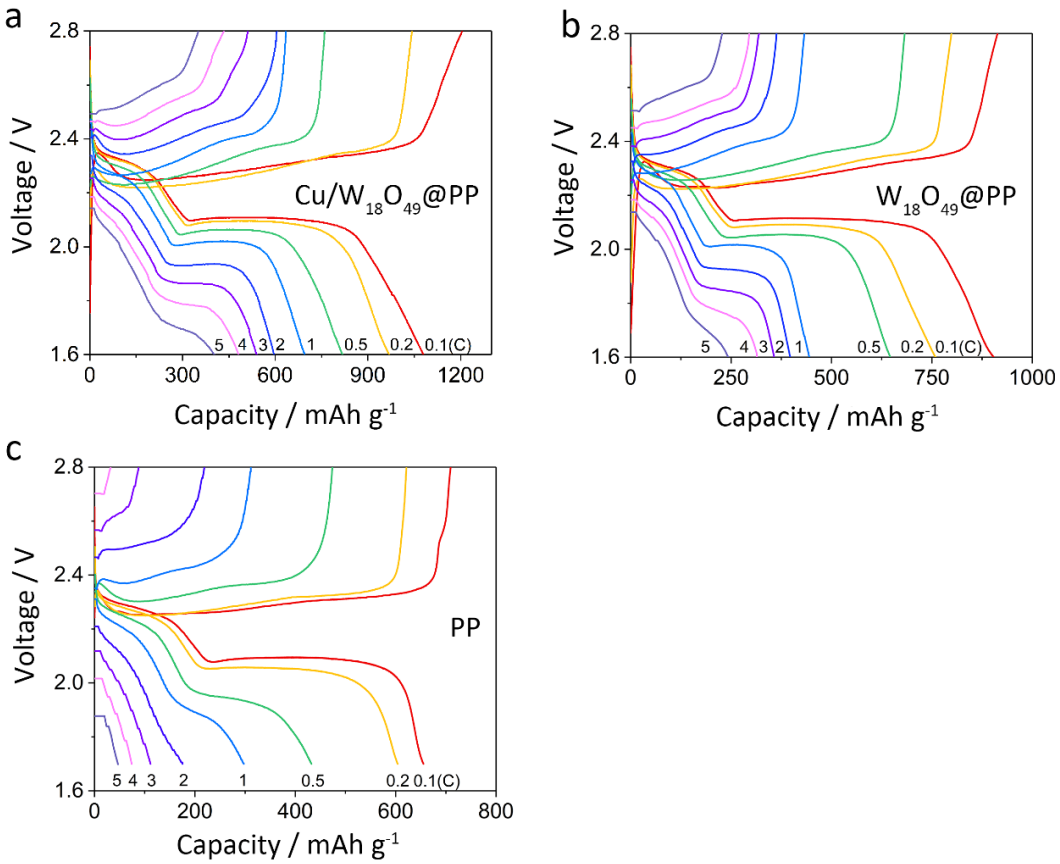

Fig. S15. Galvanostatic charge-discharge profiles of the Li//S batteries with the (a) Cu/$W_{18}O_{49}$@PP separator, (b) $W_{18}O_{49}$@PP separator and (c) PP separator.

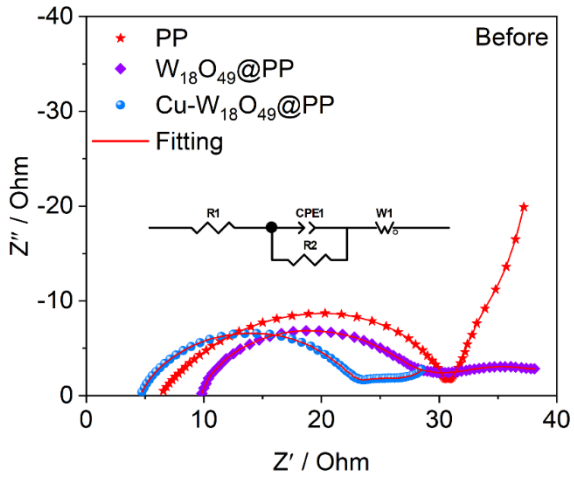

Fig. S16. EIS spectra before cycling of the Li//S batteries. The inset is the equivalent circuit for simulation.

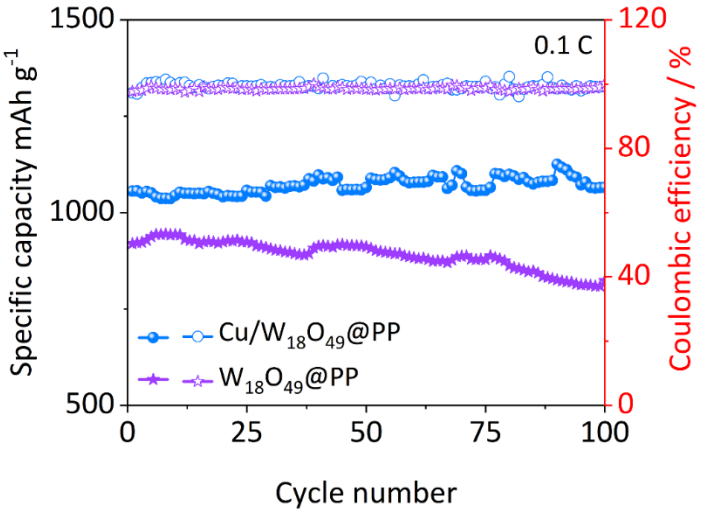

Figure S17. Cycling stability of Li//S batteries with different separators at 0.1C.

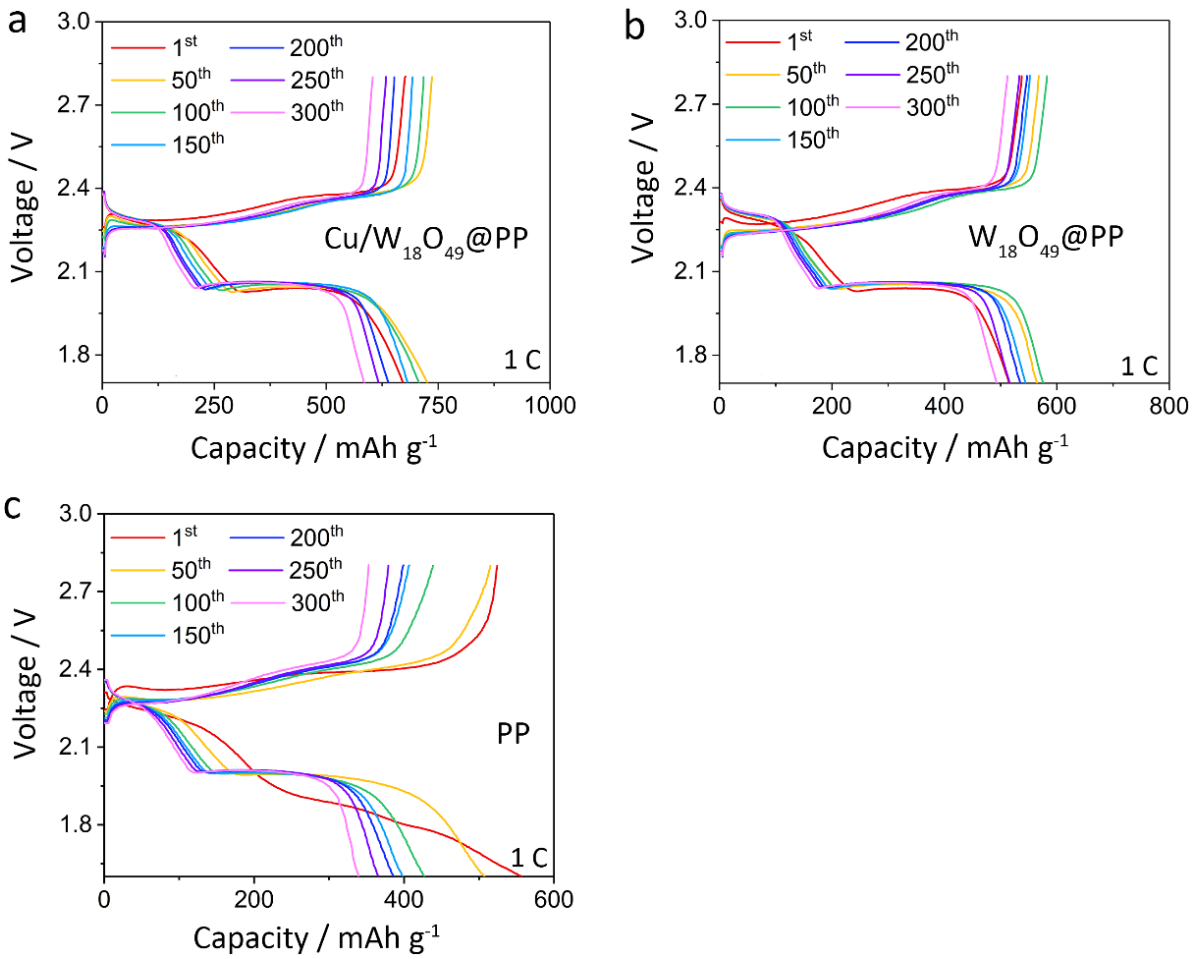

Fig. S18. Galvanostatic charge-discharge profiles of the Li//S batteries with the (a) Cu/$W_{18}O_{49}$@PP separator, (b) $W_{18}O_{49}$@PP separator and (c) PP separator.

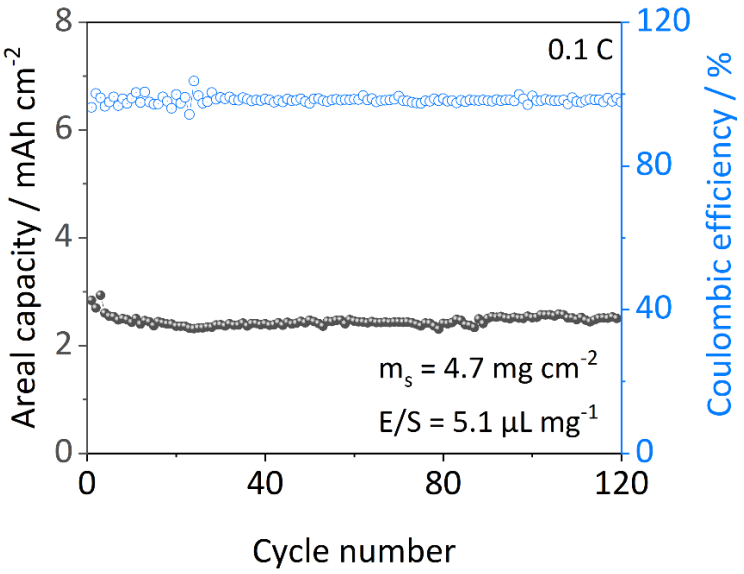

Figure S19. Cycling stability of Li//S batteries with the Cu/$W_{18}O_{49}$@PP separator, high S loading and lean electrolyte at 0.1 C.

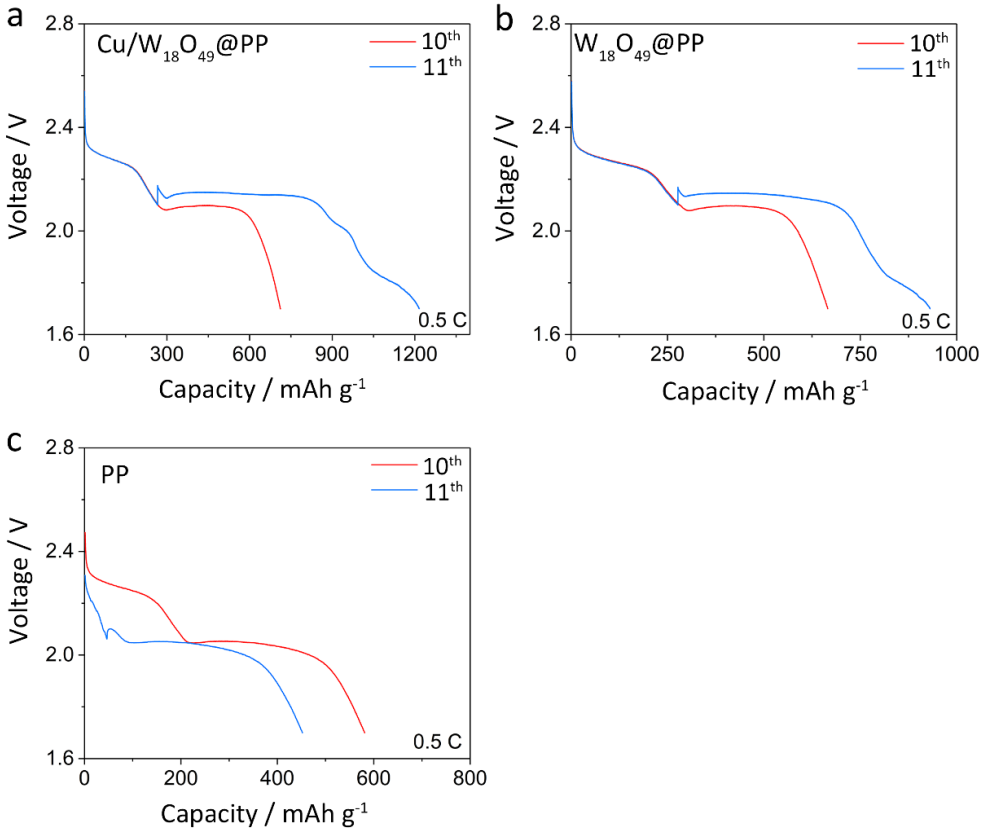

Fig. S20. Discharge curves of the 10th cycle (continuous discharge) and the 11th cycle (7d rest at 2.1 V during discharge) of the Li//S batteries with the (a) Cu/$W_{18}O_{49}$@PP separator, (b) $W_{18}O_{49}$@PP separator, and (c) PP separator.

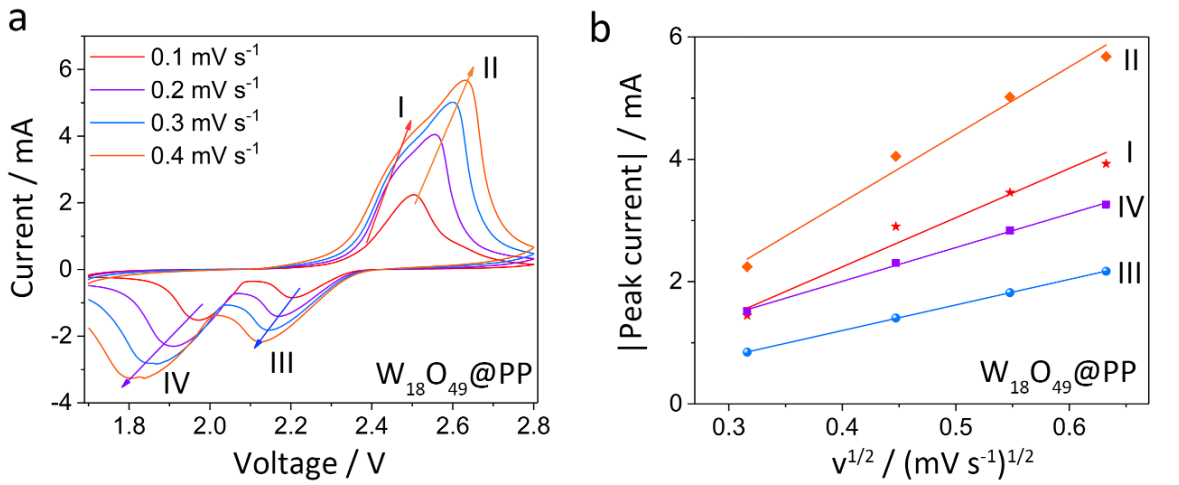

Fig. S21. (a) CV curves and (b) linear fits of the peak currents of Li//S batteries with the $W_{18}O_{49}$@PP separator.

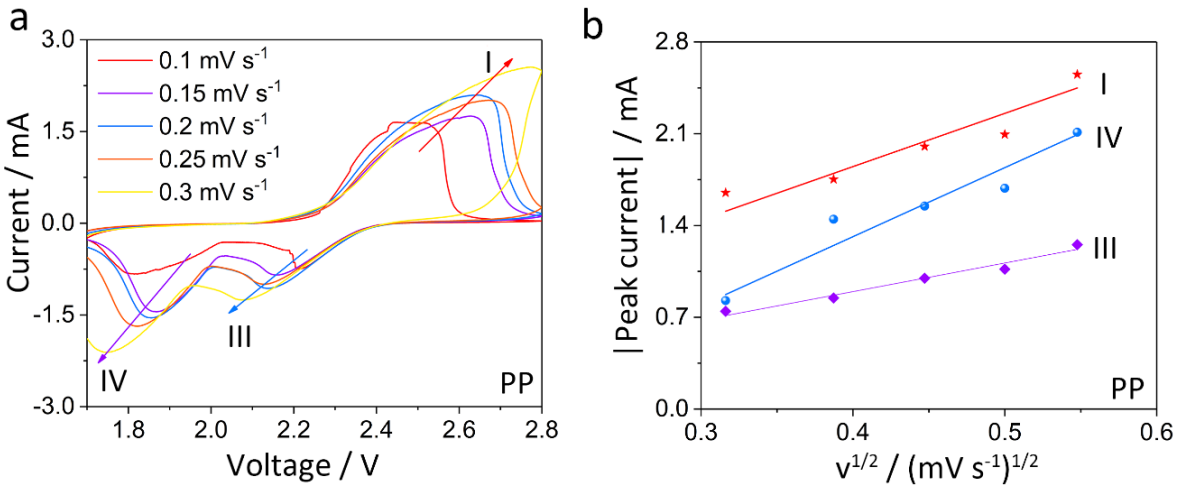

Fig. S22. (a) CV curves and (b) linear fits of the peak currents of Li//S batteries with the PP separator.

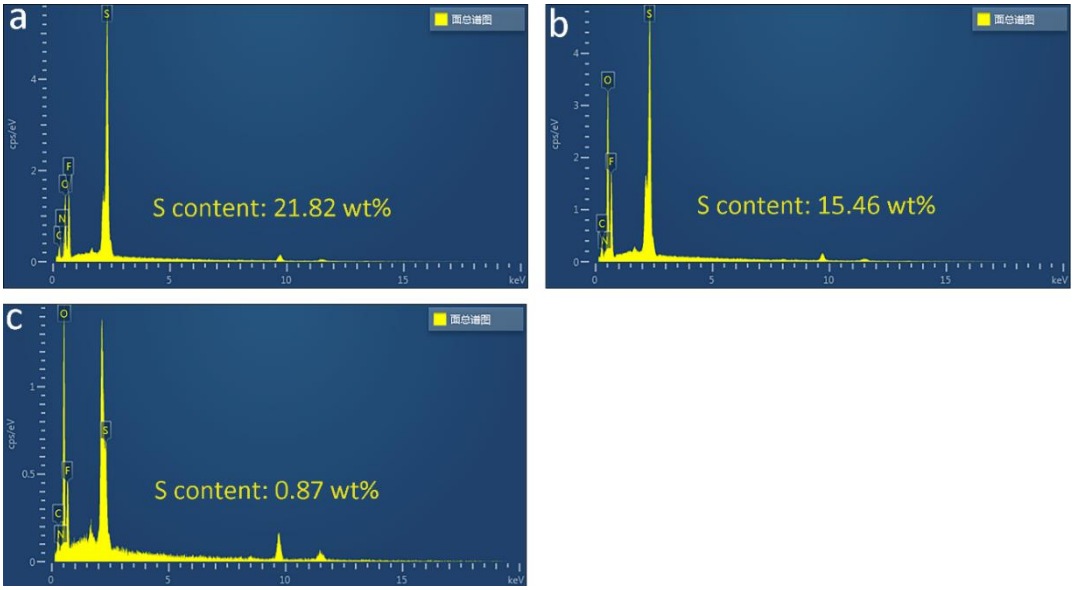

Fig. S23. EDS spectra of the cycled Li anode in the batteries with the (a) PP separator, (b) $W_{18}O_{49}$@PP separator, and (c) Cu/$W_{18}O_{49}$@PP separator.

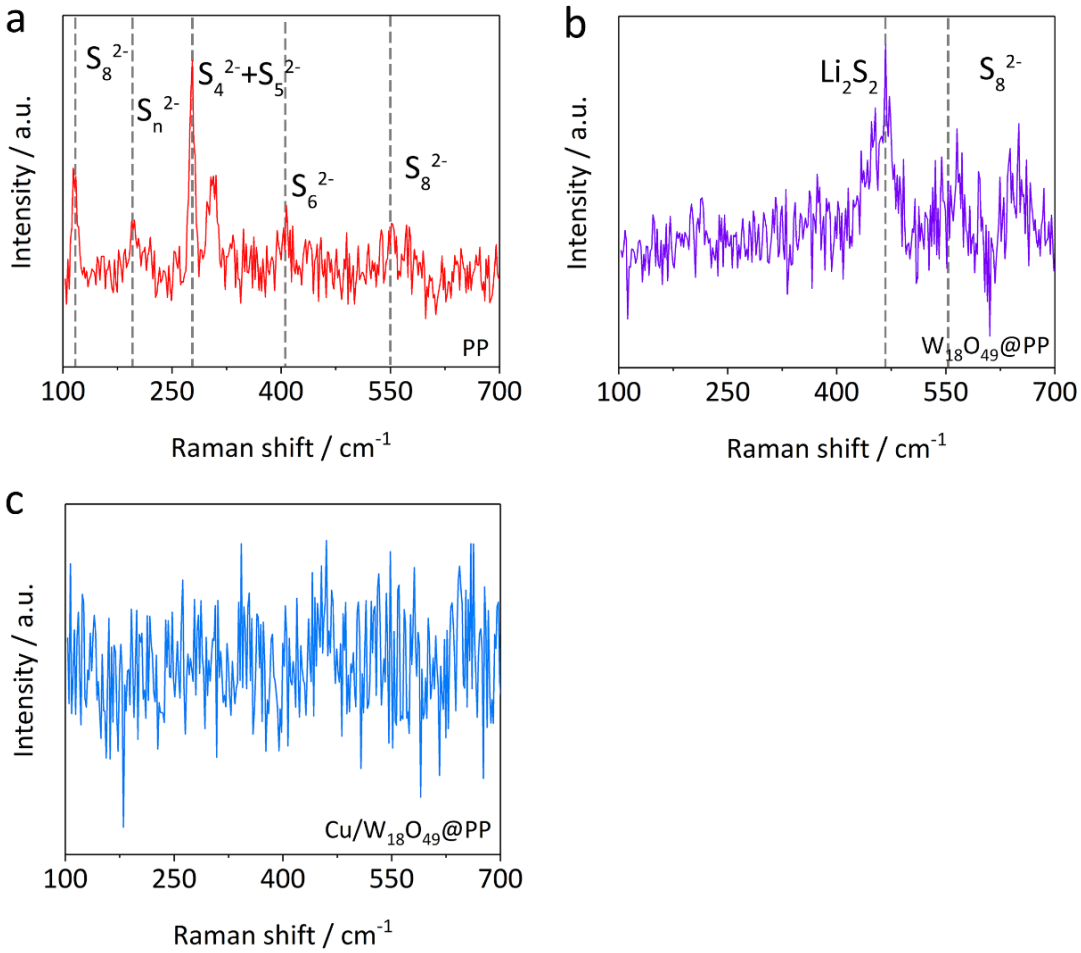

Fig. S24. Raman spectra of the cycled Li anode in the batteries with the (a) PP separator, (b) $W_{18}O_{49}$@PP separator, and (c) Cu/$W_{18}O_{49}$@PP separator.

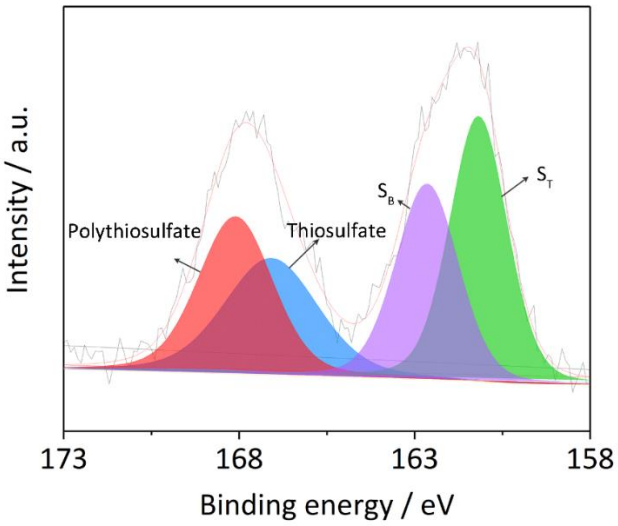

Fig. S25. High-resolution S 2p XPS spectrum of $W_{18}O_{49}$.

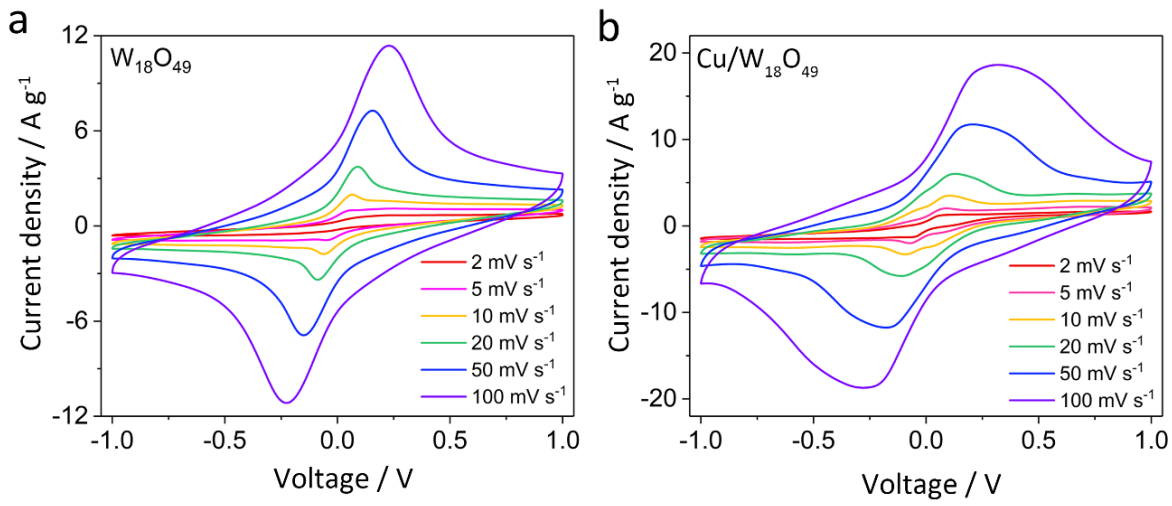

Fig. S26. CV curves of symmetric cells with the (a) $W_{18}O_{49}$ electrode and (b) $Cu/W_{18}O_{49}$ electrode under different scan rates.

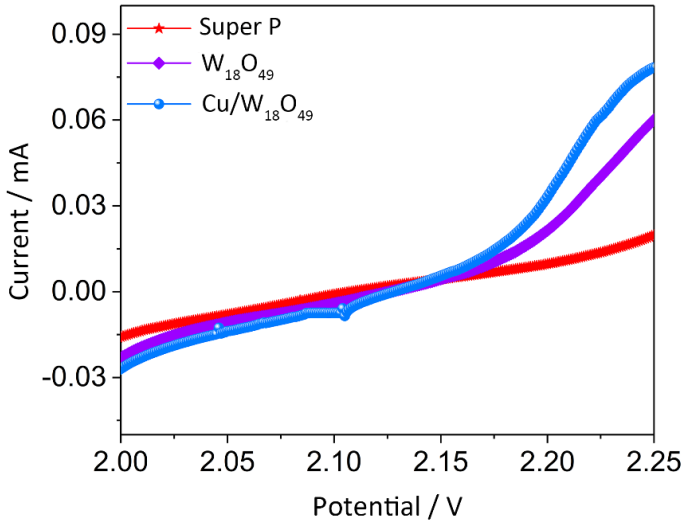

Fig. S27. Linear sweep voltammetry of cells with different electrodes.

Table S1. Comparison of properties of some representative coated separators and electrochemical performances of Li//S batteries with them.

Coating materials	Thickness of coating / μm	Ionic conductivity / mS cm^{-1}	Li^+ ion diffusion coefficient	S / wt.%	Cycling stability				Refs.
					Cycle number	Initial capacity / m Ah g^{-1}	Decaying rate / (% per cycle)	Rate / C	
$Cu/W_{18}O_{49}$	2.3	7.22	improved	64	300	687	0.046	1	**This work**
MoS_2	0.35	0.20	improved	65	600	808	0.083	0.5	[3]
BN-Carbon	13	-	-	60	250	1018.5	0.09	0.5	[4]
SnS_2@HCNF	-	-	-	64	500	1138	0.056%	1	[5]
Fe_2N/N-rGO	10	-	-	70	700	1080	0.05	1	[6]
CoFe@NC	8	-	-	70	300	889.9	0.1	0.5	[7]
RG@CoS@C	30	-	improved	65	420	-	0.08	2	[8]
Fe_3C–C/CNT	60	-	improved	-	200	-	0.1	1	[9]
Co–N_2	9.6	-	-	56	700	871	0.05	0.5	[10]
HVS	-	-	-	70	300	1156	0.072	0.2	[11]
$NiCo_2O_4$/CNF	38	0.35	-	49	500	-	0.057	2	[12]
GWF	-	-	-	64.4	200	-	0.06	1	[13]
Li-MOF/RGO	17.3	-	-	56	600	-	0.089	1	[14]

"-" mean not mentioned.

Table S2. Impedance characteristics of the Li//S batteries with different separators before cycling.

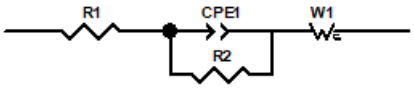

Separators	R1 / ohm	R2 / ohm
PP	9.4	24.1
$W_{18}O_{49}$@PP	6.7	16.3
Cu/$W_{18}O_{49}$@PP	4.4	15.5

Table S3. Li^+ ion diffusion coefficients of different separators.

Parameters	PP	$W_{18}O_{49}$@PP	Cu/$W_{18}O_{49}$@PP
D_{Li^+} at peak I / $cm^2\ s^{-1}$	8.05×10^{-9}	5.98×10^{-8}	6.16×10^{-8}
D_{Li^+} at peak II / $cm^2\ s^{-1}$	-	3.16×10^{-8}	7.04×10^{-8}
D_{Li^+} at peak III / $cm^2\ s^{-1}$	1.35×10^{-8}	1.49×10^{-8}	1.95×10^{-8}
D_{Li^+} at peak IV/ $cm^2\ s^{-1}$	2.32×10^{-9}	8.53×10^{-9}	3.34×10^{-8}

References

1. Y. Yang, W. Wang, L. Li, B. Li and J. Zhang, *J. Mater. Chem. A*, 2020, 8, 3692-3700
2. S. Bai, X. Liu, K. Zhu, S. Wu and H. Zhou, *Nat. Energy*, 2016, 1, 16094.
3. Z. A. Ghazi, X. He, A. M. Khattak, N. A. Khan, B. Liang, A. Iqbal, J. Wang, H. Sin, L. Li and Z. Tang, *Adv. Mater.*, 2017, 29, 1606817.
4. P. J. H. Kim, J. Seo, K. Fu, J. Choi, Z. Liu, J. Kwon, L. Hu and U. Paik, *NPG Asia Mater.*, 2017, 9, e375.
5. C. Wei, Y. Han, H. Liu, R. Gan, Q. Li, Y. Wang, P. Hu, C. Ma and J. Shi, *Carbon*, 2021, 184, 1-11.
6. X. Wang, D. Wang, C. Ma, Z. Yang, H. Yue, D. Zhang and Z. Sun, *Chem. Eng. J.*, 2022, 427, 131622.
7. Y. Wang, L. Zhu, J. Wang, Z. Zhang, J. Yu and Z. Yang, *Chem. Eng. J.*, 2021, 433, 133792.
8. J. Guo, H. Jiang, X. Li, Z. Chu, W. Zheng, Y. Dai, X. Jiang, X. Wu and G. He, *Energy Storage Mater.*, 2021, 40, 358-367.
9. S. Wang, X. Li, Y. Zhang, W. Zheng, Y. Dai and G. He, *ACS Appl. Energy Mater.*, 2020, 3, 5050-5057.
10. D. Fang, P. Sun, S. Huang, Y. Shang, X. Li, D. Yan, Y. V. Lim, C. Y. Su, B. J. Su, J. Y. Juang and H. Y. Yang, *ACS Mater. Lett.*, 2021, 4, 1-10.
11. J. Wang, S. Yi, J. Liu, S. Sun, Y. Liu, D. Yang, K. Xi, G. Gao, A. Abdelkader, W. Yan, S. Ding and R. V. Kumar, *ACS Nano*, 2020, 14, 9819-9831.
12. J. X. Lin, X. M. Qu, X. H. Wu, J. Peng, S. Y. Zhou, J. T. Li, Y. Zhou, Y. X. Mo, M. J. Ding, L. Huang and S. G. Sun, *ACS Sus. Chem. Eng.*, 2021, 9, 1804-1813.
13. Y. Chen, K. Zou, X. Dai, H. Bai, S. Zhang, T. Zhou, C. Li, Y. Liu, W. K. Pang and Z. Guo, *Adv. Funct. Mater.*, 2021, 31, 2102458.
14. M. Zhou, Y. Li, T. Lei, W. Chen, G. Rao, L. Xue, A. Hu, Y. Fan, J. Huang, Y. Hu, X. Wang and J. Xiong, *Small*, 2021, 17, e2104367.